

Intramolecular Charge and Energy Transfer Rates with Reduced Modes: Comparison to Marcus Theory for Donor-Bridge-Acceptor Systems

Xunmo Yang and Eric R Bittner*

Department of Chemistry, University of Houston, Houston, TX 77204

E-mail: bittner@uh.edu

Phone: 832-842-8849. Fax: 713-743-2709

Abstract

We present a new, fully *ab initio* approach for computing intramolecular charge and energy transfer rates. Using a time-convolutionless master equation approach and parameterized using couplings obtained using an accurate quantum chemical approach, we benchmark the approach against experimental results and Marcus theory rates for triplet energy transfer for a series of donor-bridge-acceptor systems. An important component of our analysis is the use of a projection operator scheme that parses out specific internal nuclear motions that accompany the electronic transition. Using an iterative Lanczos approach, we concentrate the coupling between the electronic and nuclear degrees of freedom into a small number of reduced harmonic modes. We find that using only a single reduced mode—termed the “primary mode”, one obtains an accurate evaluation of the golden-rule rate constant and insight into the nuclear motions responsible for coupling the initial and final electronic states. In particular, the primary mode reflects the irreducible representation of the donor and acceptor excited states.

Keywords: Quantum master equation, energy transfer rates, diabatic states, triplet energy transfer

Introduction

Energy and electronic transport plays a central role in a wide range of chemical and biological systems. It is the fundamental mechanism for transporting the energy of a absorbed photon to a reaction center in light harvesting systems and for initiating a wide range of photo-induced chemical processes, including vision, DNA mutation, and pigmentation. The seminal model for calculating electron transfer rates was developed by Marcus in the 1950's.¹⁻³

$$k_{Marcus} = \frac{2\pi}{\hbar} |V_{ab}|^2 \frac{1}{\sqrt{4\pi k_B T \lambda}} e^{-(\lambda + \Delta\epsilon)^2 / 4\lambda k_B T}. \quad (1)$$

where λ is energy required to reorganize the environment following the transfer of an electron from donor to acceptor. and $\Delta\epsilon$ is the driving force for the reaction.

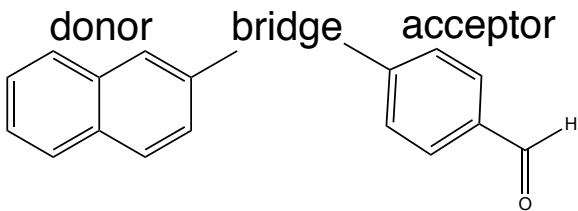
If we assume that the nuclear motions about the equilibrium configurations of the donor and acceptor species is harmonic, the chemical reactions resulting from energy or charge transfer events can be understood in terms of intersecting diabatic potentials as sketched in Fig. 1. The upper and lower curves are the adiabatic potential energy surfaces describing the nuclear dynamics resulting from an energy or charge transfer event, taking the geometry of the donor state as the origin. As the transfer occurs by crossing an energy barrier, the transfer rate can be expected to be in the Arrhenius form

$$k \propto e^{-E_A/k_B T}, \quad (2)$$

with E_A as the activation energy. Using $E_A = (\lambda + \Delta\epsilon)^2 / 4\lambda$ we can relate the activation energy to both the reorganization energy and driving force, $-\Delta\epsilon$. One of the most profound predictions of the theory is that as the driving force increases, the transfer rate reaches a maximum and further increases in the driving force lead to lower reaction rates, termed the inverted regime.

We focus here on the rates of triplet exchange between a naphthalene donor and a ben-

zaldehyde acceptor linked by a variety of bridging units.



Triplet energy exchange in these systems occurs via the through-space Dexter mechanism.⁴ This is a short-ranged interaction involving the simultaneous exchange of two electrons between the donor and acceptor moieties. Systems such as these formed the basis of a series of experiments by Closs and Miller⁵ in which they verified the existence of the Marcus inverted regime and serve as crucial benchmarks for testing new theoretical models for computing energy and charge transfer rates.^{6–8}

A number of years ago, we developed a time-convolutionless master equation approach for computing state-to-state rates in which the coupling between states depends upon the nuclear coordinates.⁹ This approach incorporates a fully quantum mechanical treatment of both the nuclear and electronic degrees of freedom and recovers well-known Marcus expression in the semiclassical limit. The model is parameterized by the vibrational normal mode frequencies, and the electronic energies and energy derivatives at a reference configuration. The approach has been used by our group to compute state-to-state transition rates in semi-empirical models for organic semiconducting light-emitting diode and photovoltaics.^{10–13} This paper represents the first time we have used this approach within the context of a fully *ab initio* quantum chemical model. As such, this present work provides an important benchmark of the approach since all parameters will be determined using state-of-the-art quantum chemical methods and results compared to both theoretical and experimental rates.

Central to the work presented here is the use of a diabatization scheme for determining donor and acceptor states in a molecular unit. We benchmark the approach by computing the triplet energy transfer rates for a series of donor-bridge-acceptor molecules originally

studied by Closs.⁵ The triplet energy transfer rates computed using our approach compare well against both the experimental rates and with more recent theoretical rates presented by Subotnik *et al.*^{6–8} An important component of our analysis is the use of a projection operator scheme that parses out specific internal nuclear motions that accompany the electronic transition. Similar decomposition schemes have been presented by Burghardt^{14–17} and the approach used here builds upon the method given in Ref. 18. By analyzing the electron-phonon couplings, we can discern a reduced set of motions that are responsible for coupling between the donor and acceptor states.

Theoretical Approach

Model Hamiltonian

We consider a generic model for n electronic states coupled linearly to a phonon bath. Taking the electronic ground state of the system as a reference and assuming that the electronic states are coupled linearly to a common set of modes, we arrive at a generic form for the Hamiltonian:

$$H = \begin{pmatrix} \epsilon_1 & 0 \\ 0 & \epsilon_2 \end{pmatrix} + \begin{pmatrix} \mathbf{g}_{11} & \mathbf{g}_{12} \\ \mathbf{g}_{21} & \mathbf{g}_{22} \end{pmatrix} \cdot \mathbf{q} + \frac{\mathbf{p}^2}{2} + \frac{1}{2} \mathbf{q}^T \cdot \boldsymbol{\Omega} \cdot \mathbf{q}. \quad (3)$$

Here, the first term contains the electronic energies, ϵ_1 and ϵ_2 computed at a reference geometry—typically that of the donor or acceptor state. The second term represents the linearized coupling between the electronic and nuclear degrees of freedom given in terms of the mass-weighted normal coordinates \mathbf{q} . The diagonal terms give the adiabatic displacement forces between the reference geometry and the two states. If we choose one of the states as the reference state, then either \mathbf{g}_{11} or \mathbf{g}_{22} will vanish. The remaining two terms correspond

Table 1: Comparison of triplet-triplet energy transfer rates obtained from our approach, Marcus rates are from Ref. 8 and experimental rates from Refs. 19,20. The experimental error is estimated to be 20% in each case studied here. The V_{ab} are the diabatic couplings obtained using Edmiston-Ruedenberg diabatization. In each case, D = 4-benzophenonyl and A = 2-naphthyl. n.r. = Not Reported.

Bridge	Structure	Rates (s^{-1})			Marcus theory parameters		
		Expt. Ref. 19,20	Marcus Theory Ref. 8	This work	λ (eV)	$\Delta\epsilon$ (eV)	V_{ab} (μeV)
c-1,3ea		3.3E9	3.9E9	2.2E9	0.823	-0.612	470.1
c-1,3ee		7.7E9	2.1E10	2.8E10	0.810	-0.580	1687.3
c-1,4ea		4.0E7	1.3E7	1.8E7	0.817	-0.604	43.20
c-1,4ee		1.3E9	3.9E9	3.6E9	0.826	-0.642	605.8
d-2,6ae		1.3E5	1.0E4	4.7E4	0.836	-0.577	2.239
d-2,6ea		7.0E5	3.9E4	5.8E4	0.821	-0.609	2.414
d-2,6ee		3.1E6	5.0E6	4.8E6	0.810	-0.581	22.12
d-2,7ae		1.1E7	2.8E7	3.0E7	0.826	-0.605	55.16
d-2,7ea		1.5E7	1.8E7	4.3E7	0.817	-0.605	65.85
d-2,7ee		9.1E7	3.5E8	3.4E8	0.831	-0.648	185.1
M		5.0E10	n.r.	1.2E9	0.896	-0.636	357.0

to the harmonic motions of the nuclear normal modes, given here in mass-weighted normal coordinates. In the normal mode basis, Ω is diagonal with elements corresponding to the normal mode frequencies, ω_j^2 .

We now separate Eq. 3 into diagonal and off-diagonal terms

$$\hat{H} = \hat{H}_o + \hat{V} \quad (4)$$

and perform a polaron transform using the unitary transformation.^{9,21,22}

$$\begin{aligned} U &= e^{-\sum_{ni} \frac{g_{nni}}{\hbar\omega_i} |n\rangle\langle n| (a_i^\dagger - a_i)} \\ &= \sum_n |n\rangle\langle n| e^{-\sum_i \frac{g_{nni}}{\hbar\omega_i} (a_i^\dagger - a_i)} \end{aligned} \quad (5)$$

under which the transformed Hamiltonian is written in terms of the diagonal elements

$$\tilde{H}_0 = U^{-1} H_0 U = \sum_n \tilde{\epsilon}_n |n\rangle\langle n| + \sum_i \omega_i a_i^\dagger a_i, \quad (6)$$

with the renormalized electronic energies,

$$\tilde{\epsilon}_n = \epsilon_n - \sum_i \frac{g_{nni}^2}{\hbar\omega_i}, \quad (7)$$

and off-diagonal terms,

$$\hat{V}_{nm} = \sum_i g_{nmi} \left(a_i^\dagger + a_i - \frac{2g_{nni}}{\hbar\omega_i} \right) e^{\sum_j \frac{(g_{nnj} - g_{mmj})}{\hbar\omega_j} (a_j^\dagger - a_j)}. \quad (8)$$

In the transformed (or dressed) picture the electronic transition from state $|n\rangle$ to $|m\rangle$ is accompanied by the excitations of all the normal phonon modes. Transforming to the interaction representation and performing a trace over the phonons gives the spectral density in terms of the autocorrelation of the electron-phonon coupling operators.

$$S_{nm}(\tilde{\omega}) = \int_{-\infty}^{\infty} dt e^{-i\tilde{\omega}t} \langle \hat{V}_{nm}(t) \hat{V}_{mn}(0) \rangle. \quad (9)$$

Here, $\hat{V}_{nm}(t)$ is the electron-phonon coupling term in the Heisenberg representation and $\langle \dots \rangle$ denotes a thermal average over the vibrational degrees of freedom. The derivation and explicit form for the kernel in Eq. 9 is quite lengthy and is given in Ref. 9.

Non-Markovian Master Equation and Golden-Rule rates

In Ref. 9, Pereverzev and Bittner derived a non-Markovian, time-convolutionless form of the Pauli master equation (TCLME) for general system described by Eq. 3.

$$\frac{dP_n}{dt} = \sum_m W_{nm}(t) P_m(t) - \left(\sum_m W_{mn}(t) \right) P_n(t) \quad (10)$$

where the time-dependent rates are given by

$$W_{nm}(\tau) = 2\text{Re} \int_0^\tau dt \left\langle \hat{V}_{nm}(0) \hat{V}_{mn}(t) \right\rangle e^{-i\tilde{\omega}_{nm} t}. \quad (11)$$

In the limit that $\tau \rightarrow \infty$, Eq. 11 gives the Fermi's Golden Rule expression for the transition rate,

$$k_{nm} = 2\text{Re} \int_0^\infty dt \left\langle \hat{V}_{nm}(0) \hat{V}_{mn}(t) \right\rangle e^{-i\tilde{\omega}_{nm} t}. \quad (12)$$

At this point it is useful to connect the various terms in the phonon-dressed Hamiltonian with specific physical parameters. First, the reorganization energy is given by

$$\lambda_{nm} = \sum_j \frac{(g_{nnj} - g_{mmj})^2}{\omega_j} = \sum_j \hbar\omega_j S_j$$

where the $\{S_j\}$ are the Huang-Rhys factors for each phonon mode. These are related to the Franck-Condon factor describing the overlap between the $v_j = 1$ vibronic state in one electronic state with the $v_j = 0$ vibronic state in the other. Likewise, the energy difference between the renormalized energy gaps is related to the driving force of the state-to-state transition,

$$\Delta E_{nm} = \tilde{\epsilon}_n - \tilde{\epsilon}_m. \quad (13)$$

The difficulty in using this approach is that it requires both diagonal (\mathbf{g}_{nn}) and off-diagonal (\mathbf{g}_{nm}) derivative couplings between adiabatic states. In the following section, we discuss how we have used the Edmiston-Ruedenberg localization scheme to estimate the couplings.²³ We also present how one can construct a reduced set of harmonic modes that fully capture the electron/nuclear coupling.

Parameterization from quantum chemistry

In order to obtain the final form of our target Hamiltonian, we assume the diabatic potentials are a good approximation to the actual adiabatic potentials.

When the adiabatic (and diabatic) energy minima are far enough away from the crossing points and the mixing angles between the diabatic and adiabatic states is small, we can use the gradients of the adiabatic potentials to approximate the diabatic potentials. Thus, if we perform calculations at the optimized geometry of the final acceptor state (*i. e.* about Q_2 in Fig. 1), we can write the Hamiltonian as

$$H_{dia,e} = \begin{pmatrix} \epsilon_1 & V_{12} \\ V_{21} & \epsilon_2 \end{pmatrix} + \begin{pmatrix} 0 & 0 \\ 0 & 1 \end{pmatrix} \mathbf{g}_{22} \cdot \mathbf{q} + H_{osc}, \quad (14)$$

where H_{osc} is the harmonic oscillator Hamiltonian for the vibrational normal modes. The linear assumption amounts to performing a series expansion of the full, multi-dimensional coupling term and keeping only the lowest order terms. Systematic improvement can be made by including higher-order (e.g. quadratic) off-diagonal couplings. However, this would involve a substantial increase in the complexity of the theory. The linear assumption is reasonable so long as the mixing angle is small, as verified by the benchmark calculations presented below.

We obtain the diabatic couplings V_{12} and the mixing angle θ via ER localization and transform the electronic Hamiltonian from the adiabatic basis to the diabatic basis *viz.*

$$H_{dia} = \begin{pmatrix} \cos \theta & -\sin \theta \\ \sin \theta & \cos \theta \end{pmatrix} \begin{pmatrix} \epsilon_1 & 0 \\ 0 & \epsilon_2 \end{pmatrix} \begin{pmatrix} \cos \theta & \sin \theta \\ -\sin \theta & \cos \theta \end{pmatrix}. \quad (15)$$

The diabatic coupling is then given by

$$V_{ab} = \frac{1}{2} \sin 2\theta (\epsilon_2 - \epsilon_1). \quad (16)$$

We then diagonalize the electronic part and transform the electron/nuclear coupling back into the adiabatic basis. In doing so, we obtain the Hamiltonian in the form given in Eq. 3

$$\begin{aligned}
 H &= U^T H_{dia} U \\
 &= \begin{pmatrix} E_1 & 0 \\ 0 & E_2 \end{pmatrix} + \begin{pmatrix} \sin^2 \theta & \frac{1}{2} \sin 2\theta \\ \frac{1}{2} \sin 2\theta & \cos^2 \theta \end{pmatrix} \mathbf{g}_{22} \cdot \mathbf{q} \\
 &+ H_{osc}.
 \end{aligned} \tag{17}$$

In Fig. 2 we show the adiabatic potential curves and off-diagonal couplings along an interpolation coordinate connecting the equilibrium geometries of the donor and acceptor states for the donor-[d-2,6ae]-acceptor case. The dashed curve gives the parabolic approximation to the lower potential curves. Along this coordinate, the off-diagonal coupling is small and essentially linear and the parabolic approximation provides a good approximation to the actual potential. This indicates that the assumptions in our model Hamiltonian are generally robust for the systems we consider herein.

Energy transfer rates in Donor-Bridge-Acceptor systems

Using the ER localization approach, all parameters needed for our model can be obtained from standard quantum chemical packages. The vertical energies, ϵ_a and ϵ_b are obtained from single point CI(S) calculations at a given reference geometry. We then project the energy gradients onto the vibrational normal coordinates to obtain the electron-phonon coupling constants. Either the Boys or ER localization scheme can be used to compute the mixing angles for constructing diabatic states. For all calculations shown here we used the qChem 4.0 code and employed the 6-31G(d)** basis set in order to compare our results with Ref. 8.

We benchmark our approach against a series of donor-bridge-acceptor molecules studied by Closs.^{19,20,24} These cases are significant in that they provided a crucial verification of the Marcus inverted regime. Table 1 and Fig. 3 summarize our results. In addition, we give

the diabatic coupling V_{ab} , reorganization energy λ , and driving force $\Delta\epsilon$ computed using the Edmiston-Reudenberg (ER) localization method.

In general, our results and those in Ref. 8 agree with each other well and both are comparable to the experimental results which report an estimated error of 10-20% in the rate for each case presented here. Furthermore, all theoretical values were computed in the absence of solvent environment, whereas the experiments were all performed in benzene solvent at a standard temperature. However, there is considerable disagreement between the experimental and theoretical results for the d-2,6ea and methyl (M) bridged cases. For the d-2,6ea bridge, our results are similar to the Marcus theory rates given in Ref. 8. In this case, the the ER localization gives a small diabatic coupling and it was difficult to obtain converged localized states. In the case of the methyl-bridge, there is a significant change in the geometry between donor and acceptor states. As a result, the potential surfaces are no longer parabolic and the Condon approximation breaks down.⁸

Determining the Optimal Electron-Phonon Coupling Components

While the Marcus expression is elegant in its simplicity in requiring three parameters that can be obtained experimentally, it masks a wealth of detail that underlie the quantum transition. Central to the theory is that there exists a collective nuclear displacement coordinate that connects the initial geometry of the donor to the final geometry of the acceptor.

Generally speaking, this collective coordinate involves all nuclear degrees of freedom. However, the form of the electronic Hamiltonian in Eq. 3 suggests that there exists a subset of motions that are specific modes that capture the majority of the electronic/nuclear coupling and give the dominant contribution to the collective reaction coordinate. Within the

linearized approximation for the electronic/nuclear coupling, we can write a force tensor

$$\mathbf{F} = \begin{pmatrix} \mathbf{g}_{11} & \mathbf{g}_{12} \\ \mathbf{g}_{21} & \mathbf{g}_{22} \end{pmatrix} \quad (18)$$

where $\mathbf{F} \cdot \mathbf{q}$ is the electronic/nuclear coupling term in Eq. 3. If we consider each unique element $\{\mathbf{g}_{11}, \mathbf{g}_{12}, \mathbf{g}_{22}\}$ to be linearly independent, but non-orthogonal force vectors, one can develop a projection operator scheme to parse the N -dimensional linear vector space spanned by the mass-weighted normal mode vectors into two subspaces: one spanned by three vectors describing the coupling between the electronic states and the other spanned by the remaining $N - 3$ dimensional space spanned by motions that do not couple the electronic states. This subspace can be generated by defining a projection operator

$$\mathbf{P} = \sum'_{\alpha\beta} (\mathbf{S}^{-1})_{\alpha\beta} \mathbf{g}_\alpha \otimes \mathbf{g}_\beta \quad (19)$$

in which the summation is limited to linearly independent vectors. Here $\mathbf{S}_{\alpha\beta} = \mathbf{g}_\alpha \cdot \mathbf{g}_\beta$, \otimes is outer product, and \mathbf{I} is unitary operator. This $N \times N$ matrix projects out all normal modes that are directly coupled to the electronic degrees of freedom and its complement $\mathbf{Q} = \mathbf{I} - \mathbf{P}$ projects out all modes not directly coupled. By diagonalizing the matrix

$$\mathbf{K} = \mathbf{P} \cdot \boldsymbol{\Omega} \cdot \mathbf{P} + \mathbf{Q} \cdot \boldsymbol{\Omega} \cdot \mathbf{Q} \quad (20)$$

we obtain a transformation, \mathbf{M} , between the normal coordinates and a new set of orthogonal coordinates. Both $\mathbf{P} \cdot \boldsymbol{\Omega} \cdot \mathbf{P}$ and $\mathbf{Q} \cdot \boldsymbol{\Omega} \cdot \mathbf{Q}$ are $N \times N$ matrices. However, for a two-state system, the former will have exactly 3 non-trivial eigenvalues, $\{\alpha_p\}$, with corresponding eigenvectors, $\{M_p\}$, whereas the latter will have exactly $N_r = N - 3$ non-trivial eigenvalues, $\{\alpha_q\}$, and corresponding eigenvectors, $\{M_q\}$. This the full $N \times N$ transformation is formed by joining the non-trivial vectors from the two respective subspaces $\mathbf{M} = \{M_p, M_q\}$. The

transformed electron-phonon coupling constants are given by projecting the couplings in the normal mode basis on to the new basis.

$$\mathbf{g}'_{ab} = \mathbf{M}_p \cdot \mathbf{g}_{ab}. \quad (21)$$

By examining the types of molecular motions that compose the \mathbf{M}_p subspace, we can gain a deeper understanding of the specific classes of internal motion that are directly involved with the electron transfer process. In addition, we can gain a computational advantage since presumably this reduced set of modes give the dominant contribution to the electron-phonon coupling and autocorrelation function given as the kernel in Eq. 12.

Lanczos Method

It is crucial to notice that the vectors given in Eq. 17 are *not linearly independent*. Consequently, special care must be taken to generate the reduced sub-space. To do so, we use an iterative Lanczos approach taking the normalized vector $\mathbf{v}_1 = \mathbf{g}_{22}$ as a starting point.

As above, we initialize each step indexed by k , by defining a projection operator

$$\mathbf{P}_k = \mathbf{v}_k \otimes \mathbf{v}_k \quad (22)$$

and its complement $\mathbf{Q}_k = \mathbf{I} - \mathbf{P}_k$. k -th mode. We then project the hessian matrix $\boldsymbol{\Omega}$ into each subspace *viz.*

$$\boldsymbol{\Omega}_p = \mathbf{P}_k \cdot \boldsymbol{\Omega} \cdot \mathbf{P}_k \quad \& \quad \boldsymbol{\Omega}_q = \mathbf{Q}_k \cdot \boldsymbol{\Omega} \cdot \mathbf{Q}_k \quad (23)$$

and diagonalize each to obtain eigenvalues and eigenvectors $\{\alpha_p, \mathbf{M}_p\}$ and $\{\alpha_q, \mathbf{M}_q\}$ respectively. As above, $\boldsymbol{\Omega}_p$ and $\boldsymbol{\Omega}_q$ are $N \times N$ matrices. The first set will have a single non-trivial eigenvalue and the second set will have $N - k$ non-trivial eigenvalues. As above we collect the

non-trivial eigenvectors associated with each to form the orthogonal transformation matrix

$$\mathbf{M}_k = \{\mathbf{M}_p, \mathbf{M}_q\}. \quad (24)$$

and again transform the full hessian Ω into this new vector space to form the $N \times N$ matrix Ω' . At each step in the iteration, the transformed hessian, Ω' is in the form of a $k \times k$ tri-diagonal submatrix in the upper-left part of the matrix and a diagonal submatrix in the lower-right. For example, after $k = 3$ iterations, one has a Hessian matrix of the form:

$$\Omega' = \begin{pmatrix} \alpha_1 & b_1 & 0 & & & & 0 \\ b_1 & \alpha_2 & b_2 & & & & \\ 0 & b_2 & \alpha_3 & c_{k+1} & c_{k+2} & \cdots & c_N \\ & c_{k+1} & \alpha_{k+1} & & & & 0 \\ & c_{k+2} & & \alpha_{k+2} & & & \\ & \vdots & & & \ddots & & \\ 0 & c_N & 0 & & & & \alpha_N \end{pmatrix}. \quad (25)$$

We note that only the k -th mode is coupled the $N - k$ remaining modes. Since all of the transformations are orthogonal, diagonalizing Ω' at any point returns the original Hessian matrix.

To continue iterating, we take the k -th row of Ω' and zero the first k elements

$$\mathbf{e} = \{0, \dots, 0, c_{k+1}, c_{k+2}, \dots, c_N\}.$$

This is the coupling between the upper tridiagonal block and the lower diagonal block. We thus obtain a new vector

$$\mathbf{v}_{k+1} = \mathbf{e} \cdot \mathbf{M}$$

which is then reintroduced into the iteration scheme.

At any point along the way, we can terminate the iteration and obtain a reduced set of couplings. Since the Lanczos approach uses the power method for finding the largest eigenvector of a matrix, it converges first upon the vector with the largest electron/nuclear coupling—which we refer to as the “primary mode”. Subsequent iterations produce reduced modes with weaker electron/nuclear couplings and the entire process can be terminated after a few iterations. After k -steps, the final electron-phonon couplings are then obtained by projecting the original set of couplings (in the normal mode basis) into the final vector space.

For the first iteration, \mathbf{v}_1 is parallel to the bare electron-phonon coupling vector g_{22} and the associated frequency is $\mathbf{v}_1 \cdot \Omega \cdot \mathbf{v}_1$. The subsequent iterations introduce corrections to this via phonon-phonon coupling. For example, for the $k = 3$ iteration, we would determine the active vector space in terms of the upper-left 3×3 block of the matrix in Eq. 25.

$$\boldsymbol{\Omega}'_3 = \begin{pmatrix} \alpha_1 & b_1 & 0 \\ b_1 & \alpha_2 & b_2 \\ 0 & b_2 & \alpha_3 \end{pmatrix} \quad (26)$$

Diagonalizing $\boldsymbol{\Omega}'_3$ returns a set of frequencies and associated eigenvectors which are then used to compute the electron-phonon couplings in this reduced active space. After $N - 1$ iterations, $\boldsymbol{\Omega}'$ is a fully tridiagonal matrix and diagonalizing this returns the original normal mode basis.

As an illustrative example of our approach, we consider the first few collective modes for the c-1,4ee and d-2,5ae cases. In Fig. 4 we show the projection of the primary coupling mode onto the coordinate frame of each molecule. The vectors indicate the direction of the electron-phonon coupling vectors projected onto the Cartesian displacement vectors of the individual atoms. In each case, the primary coupling mode involves the b_{2u} in plane C=C stretching motions of the naphthalene donor and the in-plane ν_8 (in the Mulliken numbering scheme) ring-squeezing motions of the benzaldehyde acceptor.²⁵ It is interesting to note that

$^3B_{2u}$ is also the symmetry of the first triplet $\pi - \pi^*$ excited state in naphthalene.²⁶ Moreover, if we were to approximate benzaldehyde as a C_{2v} molecule, taking the aldehyde as local site, the resulting first triplet $\pi - \pi^*$ is the product of a b_1 HOMO and a b_1 LUMO giving a state in the a_1 irreducible representation. This is the same irreducible representation one obtains for the ν_8 mode, approximating it as a symmetric stretching mode. This suggests the existence of underlying symmetry selection or propensity rule in determining the coupling modes.

In order to substantiate our claim that the reduced modes generated by the iterative procedure capture the most important electron-phonon couplings, we consider the convergence of the electron-phonon autocorrelation function used to compute the golden-rule rate constants

$$C(t) = \langle \hat{V}_{nm}(t) \hat{V}_{nm}(0) \rangle \quad (27)$$

with respect to the number of reduced modes. We can this term exactly using all N vibrational modes of the molecule and compare to the results obtained using a subset of modes.

In Fig. 5 we examine the convergence of $C(t)$ with respect to number of reduced modes for the c-1,4ee and d-2,6ae cases. In both cases, only a handful of reduced modes (4 for c-1,4ee and 15 for d-2,6ae) is needed to accurately track the correlation function for the first 10 fs. For comparison, d-2,6ae has 162 normal modes and c-1,4ee has 132 normal modes. For the primary mode approximation, the recursions appear every 23 fs and are suppressed by the addition of more reduced modes to the calculation. The 23 fs recursion time corresponds to the period of the single reduced mode: $\omega_1 = 0.18\text{eV}$ (1450 cm^{-1}). For the d-2,6ae case, including 15 modes is sufficient to fully suppress the recursion time to beyond 100 fs. For purposes of computing golden rule rate constants, the Markov limit is reached when $C(t) \rightarrow 0$. For the cases at hand, this is well before the first recursion seen in Fig. 5.

While it is surprising that only a few reduced modes are needed to converge the coupling correlation function, only a single mode is necessary to accurately compute the golden-rule

rate constant. In Fig. 6 we compare the exact rate constant (using all modes) and rate constants computed using only the first mode generated by the Lanczos iterations. In the first case represented by the blue points, we approximate the reorganization energy as

$$\lambda_{nm} \approx \frac{g_1^2}{\omega_1}$$

where g_1 and ω_1 are the coupling and frequency of the first reduced mode. This simple approximation does a superb job compared to the numerically exact rate obtained using all modes and all couplings. On average, the error between the exact and approximate rate is 2% over the entire series of model donor-bridge-acceptor systems considered. The red points represent rates computed using the first reduced mode, but use the exact reorganization energy. Here, the agreement is almost perfect for the two fastest rates corresponding to d-2,6ae and d-2,6ea. However, on average this approximation is off by a factor of 3 compared to the exact rate. For the methyl-bridged case, the rate is off by a factor of 8.. This implies that the first reduced mode indeed captures the majority of the electron-phonon coupling and provides a unique description of the Marcus reaction coordinate.

In Table 2 we tabulate the frequencies and electron-phonon coupling constant for the first reduced mode for each test case. Uniformly, these modes correspond to ring breathing motions on the donor and acceptor as illustrated in Fig. 4. As seen in this figure, coupling mode does not involve normal modes localized on the bridge species. Moreover, the magnitude of the electronic coupling carried by this mode is uniformly around 0.37 eV and independent of the bridge. No single normal mode captures all of the electronic coupling. This is evidenced by the fact that the magnitude of the electronic coupling carried by the first reduced mode is over twice that of the largest coupling along a single normal mode.

Table 2: Frequencies and dimensionless electron-phonon couplings for the first reduced mode for each model system. The last column gives the absolute value of the largest coupling constant within the normal mode basis.

bridge	ω_1 (eV)	$ g_1 $ (eV)	$ g_{max} $ (eV)
c-1,3ea	0.184	0.367	0.159
c-1,3ee	0.185	0.365	0.162
c-1,4ea	0.185	0.367	0.166
c-1,4ee	0.185	0.370	0.171
d-2,6ae	0.185	0.367	0.159
d-2,6ea	0.185	0.367	0.142
d-2,6ee	0.185	0.365	0.143
d-2,7ae	0.184	0.366	0.165
d-2,7ea	0.185	0.367	0.142
d-2,7ee	0.185	0.370	0.149
M	0.184	0.366	0.160

Discussion

We present here a new approach for computing intramolecular energy and charge transfer rates by combining a time-convolutionless master equation approach for state to state population transfer as parameterized by a rigorous quantum chemical approach. The approach is robust over a wide range of model systems and generally gives good agreement compared to experimental rates and Marcus theory rates. Only in cases where the parabolic approximation to the diabatic potentials breaks down or when the ER localization method fails to converge is the agreement with the experimental rates less than satisfactory.

A crucial part of our analysis is the identification of a subset of collective modes that contain the electron-phonon couplings. Moreover, we show that there exists a unique mode—the “primary mode”, determined via an iterative approach, along which the off-diagonal electron-phonon coupling is maximized. Using only the primary mode mode as input to our golden-rule rate expression, we obtain excellent agreement (to within 2% on average over all of the donor-bridge-acceptor systems studied here) when compared to an exact evaluation using all normal modes. One can visualize the primary mode by projecting it on to the nuclear displacement vectors and gain insight into the coupled electronic/nuclear motions

that underlie an electronic transition. Our analysis also suggests that the primary mode reflects the irreducible representations of the donor and acceptor excited states.

Acknowledgement

ERB acknowledges support from the National Science Foundation (CHE-1362006), and the Robert A. Welch Foundation (E-1337). We specifically thank Prof. Joseph Subotnik and his group for discussions pertaining to the use of the ER localization methods and their implementation in qChem. XY thanks Nadia El-Hamdi for inspiration.

References

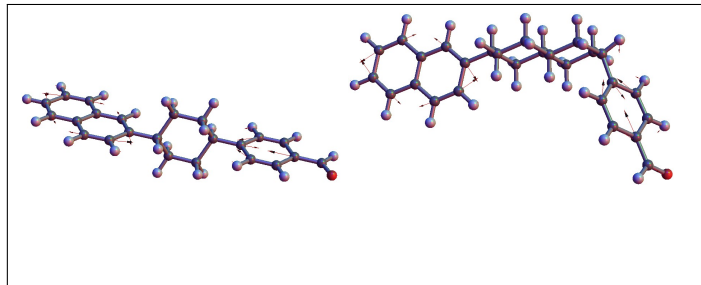
- (1) Marcus, R. A. On the Theory of Oxidation-Reduction Reactions Involving Electron Transfer. I. *J. Chem. Phys.* **1956**, *24*, 966–978.
- (2) Marcus, R. A. On the Theory of Electron-Transfer Reactions. VI. Unified Treatment for Homogeneous and Electrode Reactions. *J. Chem. Phys.* **1965**, *43*, 679.
- (3) Marcus, R. A. Electron transfer reactions in chemistry. Theory and experiment. *Rev. Mod. Phys.* **1993**, *65*, 599–610.
- (4) Dexter, D. L. A Theory of Sensitized Luminescence in Solids. *J. Chem. Phys.* **1953**, *21*, 836–850.
- (5) Miller, J.; Calcaterra, L.; Closs, G. Intramolecular long-distance electron transfer in radical anions. The effects of free energy and solvent on the reaction rates. *J. Am. Chem. Soc.* **1984**, *106*, 3047–3049.
- (6) Subotnik, J. E.; Yeganeh, S.; Cave, R. J.; Ratner, M. A. Constructing diabatic states from adiabatic states: Extending generalized Mulliken–Hush to multiple charge centers with Boys localization. *J. Chem. Phys.* **2008**, *129*, 244101.

- (7) Subotnik, J. E.; Cave, R. J.; Steele, R. P.; Shenvi, N. The initial and final states of electron and energy transfer processes: Diabatization as motivated by system-solvent interactions. *J. Chem. Phys.* **2009**, *130*, 234102–234102.
- (8) Subotnik, J. E.; Vura-Weis, J.; Sodt, A. J.; Ratner, M. A. Predicting accurate electronic energy transfer rates via Marcus theory and Edmiston-Ruedenberg localized diabatization. *J. Phys. Chem. A* **2010**, *114*.
- (9) Pereverzev, A.; Bittner, E. R. Time-convolutionless master equation for mesoscopic electron-phonon systems. *J. Chem. Phys.* **2006**, *125*, 104906.
- (10) Tamura, H.; Ramon, J. G. S.; Bittner, E. R.; Burghardt, I. Phonon-Driven Ultrafast Exciton Dissociation at Donor-Acceptor Polymer Heterojunctions. *Physical Review Letters* **2008**, *100*, APS.
- (11) Tamura, H.; Bittner, E. R.; Burghardt, I. Exciton dissociation at donor-acceptor polymer heterojunctions: Quantum nonadiabatic dynamics and effective-mode analysis. *J. Chem. Phys.* **2007**, *126*, 021103.
- (12) Bittner, E. R.; Silva, C. Noise-induced quantum coherence drives photo-carrier generation dynamics at polymeric semiconductor heterojunctions. *Nat. Comm.* **2014**, *5*, 3119.
- (13) Singh, J.; Bittner, E. R.; Beljonne, D.; Scholes, G. D. Fluorescence Depolarization in MEH-PPV: Sites vs. Eigenstates Hopping. *J. Chem. Phys.* **2009**, *131*, 194905.
- (14) Cederbaum, L.; Gildensperger, E.; Burghardt, I. Short-Time Dynamics Through Conical Intersections in Macrosystems. *Phys. Rev. Lett.* **2005**, *94*, 113003.
- (15) Gindensperger, E.; Burghardt, I.; Cederbaum, L. S. Short-time dynamics through conical intersections in macrosystems. I. Theory: Effective-mode formulation. *J. Chem. Phys.* **2006**, *124*, 144103.

- (16) Gindensperger, E.; Burghardt, I.; Cederbaum, L. S. Short-time dynamics through conical intersections in macrosystems. II. Applications. *J. Chem. Phys.* **2006**, *124*, 144104.
- (17) Cederbaum, L. S.; Gindensperger, E.; Burghardt, I. Short-Time Dynamics Through Conical Intersections in Macrosystems. *Phys. Rev. Lett.* **2005**, *94*, 113003.
- (18) Pereverzev, A.; Bittner, E. R.; Burghardt, I. Energy and charge-transfer dynamics using projected modes. *J. Chem. Phys.* **2009**, *131*, 034104.
- (19) Closs, G. L.; Piotrowiak, P.; MacInnis, J. M.; Fleming, G. R. Determination of long-distance intramolecular triplet energy-transfer rates. Quantitative comparison with electron transfer. *J. Am. Chem. Soc.* **1988**, *110*, 2652–2653.
- (20) Closs, G. L.; Johnson, M. D.; Miller, J. R.; Piotrowiak, P. A connection between intramolecular long-range electron, hole, and triplet energy transfers. *J. Am. Chem. Soc.* **1989**, *111*, 3751–3753.
- (21) Grover, M. K.; Silbey, R. Exciton–Phonon Interactions in Molecular Crystals. *J. Chem. Phys.* **1970**, *52*, 2099–2108.
- (22) Rice, M. J.; Gartstein, Y. N. Excitons and interband excitations in conducting polymers based on phenylene. *Phys. Rev. Lett.* **1994**, *73*, 2504–2507.
- (23) Edmiston, C.; Ruedenberg, K. Localized Atomic and Molecular Orbitals. *Rev. Mod. Phys.* **1963**, *35*, 457–464.
- (24) Closs, G. L.; Miller, J. R. Intramolecular long-distance electron transfer in organic molecules. *Science* **1988**, *240*, 440–447.
- (25) Silva, C. R.; Reilly, J. P. Theoretical Calculations on Excited Electronic States of Benzaldehyde and Observation of the $S_2 \leftarrow S_0$ Jet-Cooled Spectrum. *J. Phys. Chem.* **1996**, *100*, 17111–17123.

- (26) Ågren, H.; Minaev, B. F.; Knuts, S. Response Theory Studies of Triplet-State Spectra and Radiative Lifetimes of Naphthalene, Quinoxaline, and Phthalazine. *J. Phys. Chem.* **1994**, *98*, 3943–3949.

Graphical TOC Entry



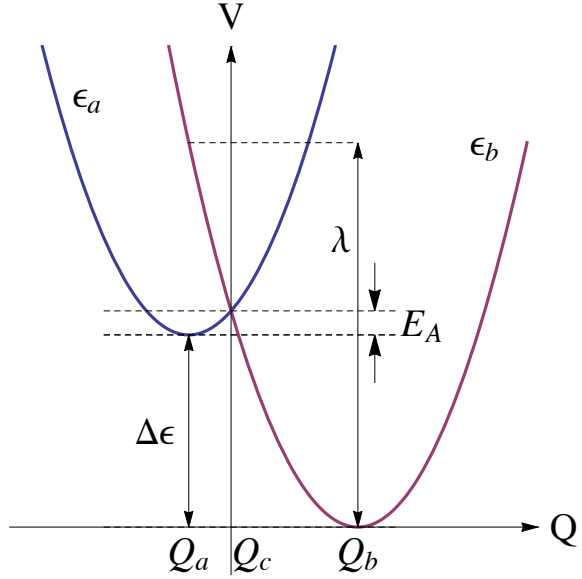


Figure 1: Sketch of Marcus parabolas for a model energy or charge transfer system. Labeled are the key parameters used to compute the Marcus rate constant (Eq. 1). Energies are given in eV and the collective nuclear displacement is dimensionless.

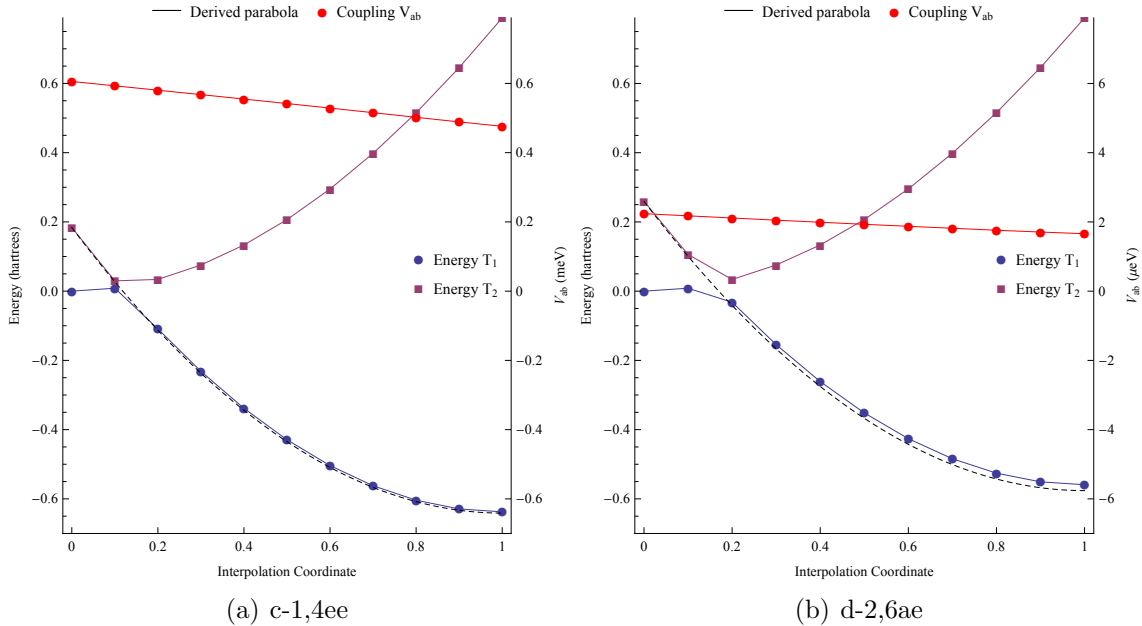


Figure 2: Adiabatic energy curves and off-diagonal couplings computed along an interpolation coordinate between the $D^* - B - A$ and $D - B - A^*$ equilibrium geometries. V_{ab} is the off-diagonal coupling at each point along this coordinate.

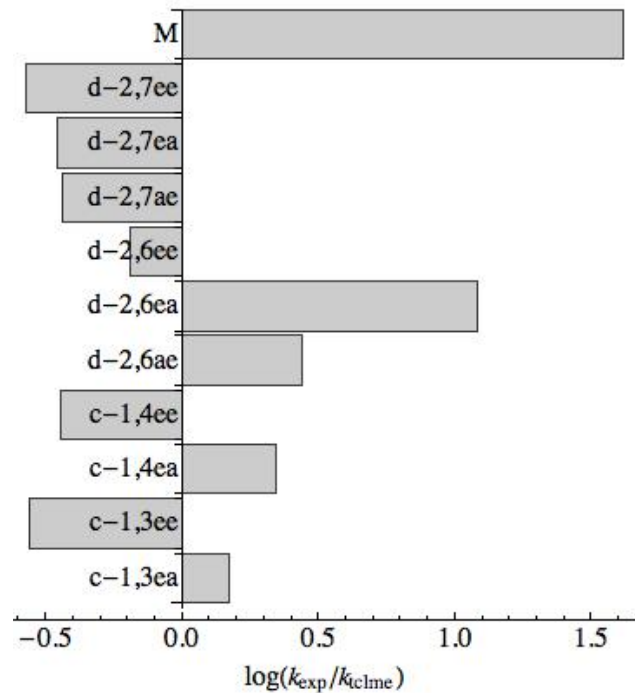


Figure 3: Comparison between predicted (TCLME) rate constants and the experimental rates from Ref. 5. With exception of the methyl and D-2,6-ea bridged cases, the TCLME results are in good agreement with the experimental results.

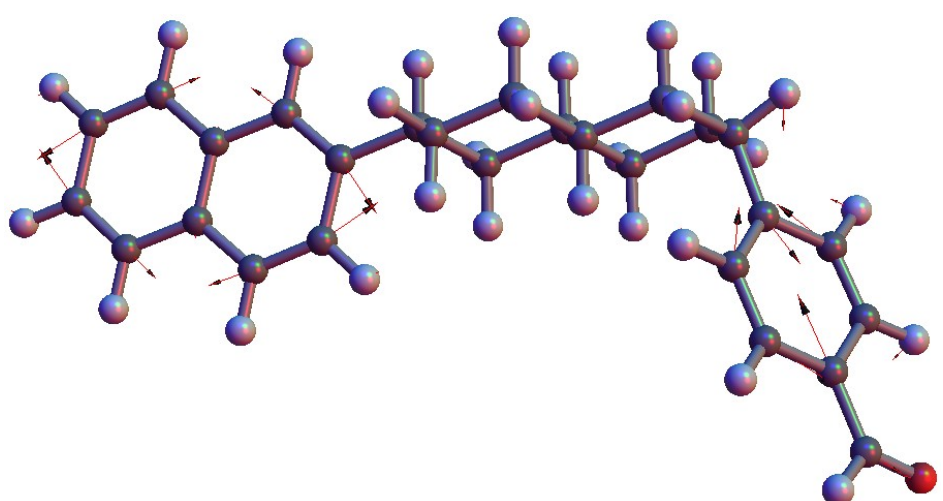
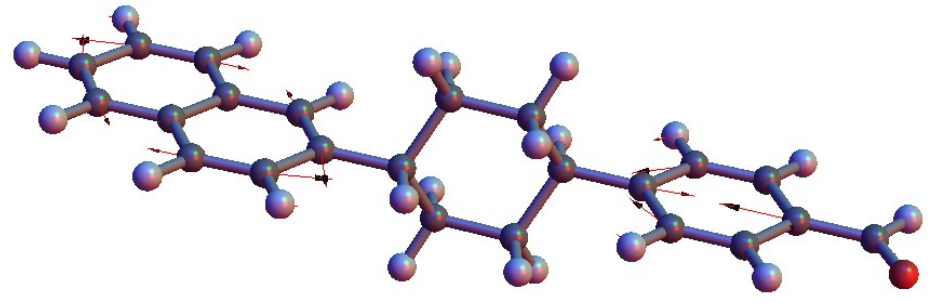


Figure 4: Primary coupling modes for (a) c-1,4ee and (b) d-2,6ae projected onto the atomic displacement coordinates.

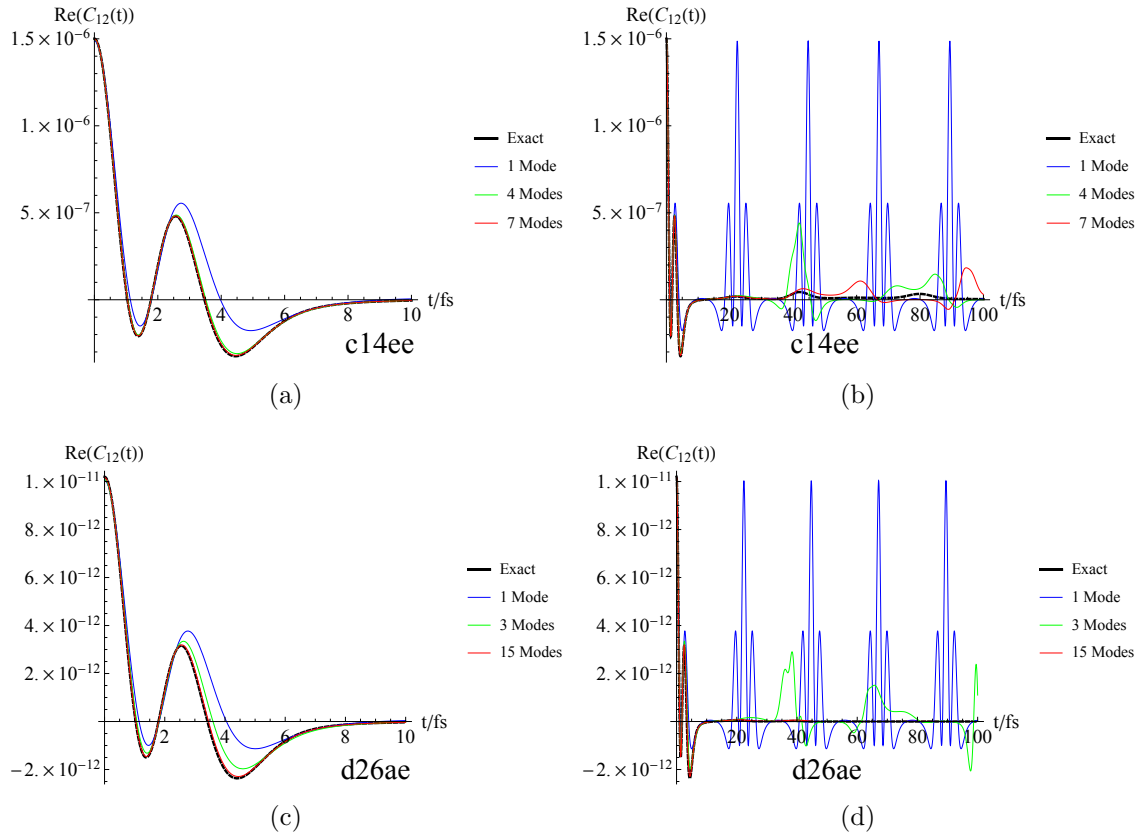


Figure 5: Convergence of the electronic coupling autocorrelation function (Eq. 27) with respect to number of reduced modes.

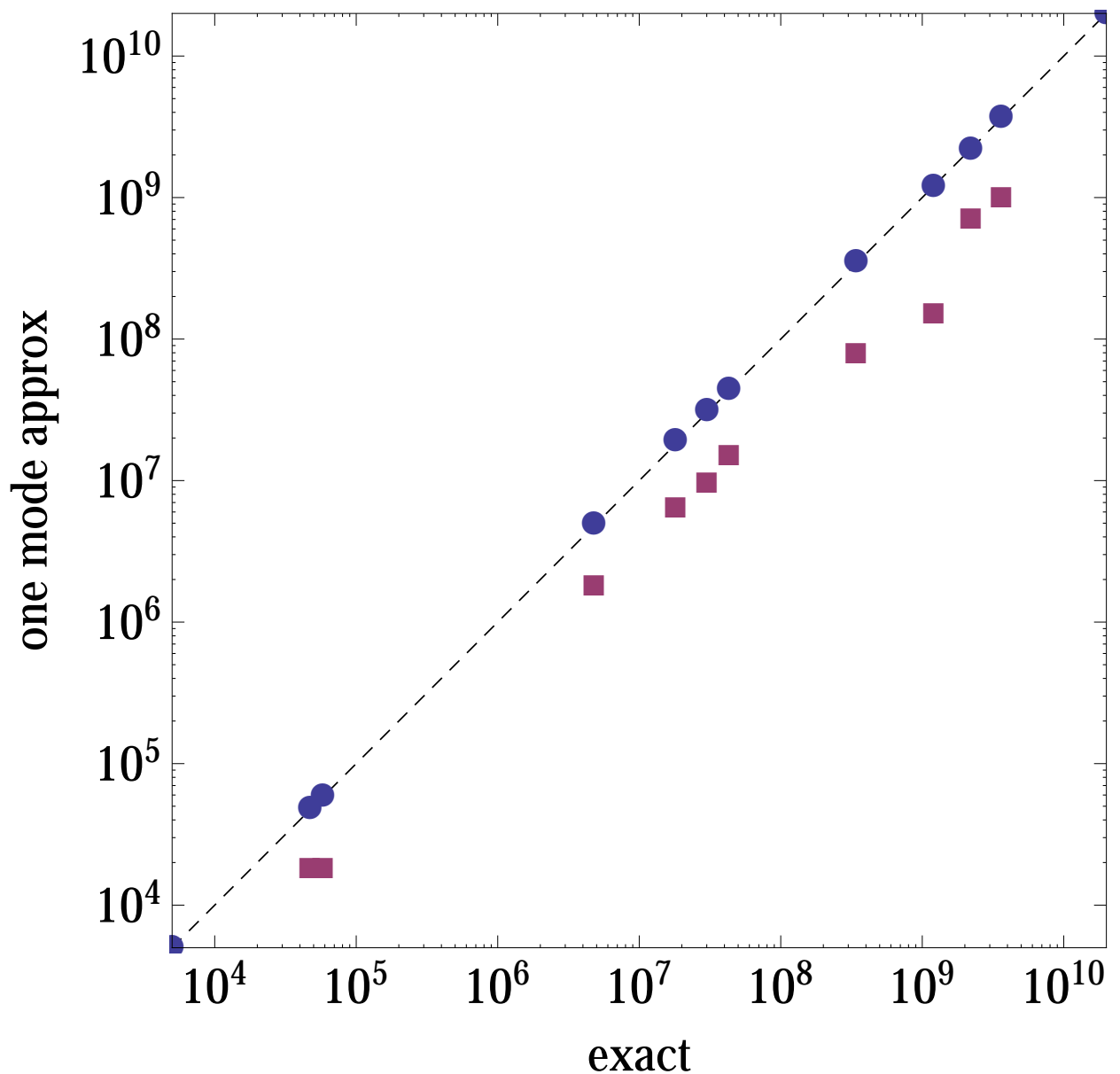


Figure 6: Comparison between exact rate constant and its primary mode approximation. The blue points correspond to rates computed using only the primary mode and the reorganization energy for only that mode. The red points use the primary mode and the exact renormalized energies.